

1 A Spatial Markov Model for upscaling transport of
2 adsorbing-desorbing solutes

3 Thomas Sherman^a, Amir Paster^c, Giovanni Porta^b, Diogo Bolster^a

4 ^a*Dept. of Civil and Environmental Engineering and Earth Sciences, University of Notre*
5 *Dame, IN, USA*

6 ^b*Dipartimento Ingegneria Civile ed Ambientale Politecnico di Milano, Piazza L. Da*
7 *Vinci, 32, 20133 Milano, Italy*

8 ^c*BreezoMeter, Haifa, Israel*

9 **Abstract**

10 The Spatial Markov Model (SMM) is an upscaled model with a strong
11 track record in predicting upscaled behavior of conservative solute transport
12 across hydrologic systems. Here we propose an SMM that can account for
13 reactive linear adsorption and desorption processes and test it on a simple
14 benchmark problem: flow and transport through an idealized periodic wavy
15 channel. The methodology is built using trajectories that are obtained from
16 a single high resolution random walk simulation of conservative transport
17 across one periodic element. Our approach encodes information about where
18 a particle starts at the inlet, where it leaves at the outlet, how long it takes
19 to cross the domain and one additional piece of information, the number of
20 times a particle strikes the boundary, with the objective of predicting large
21 scale transport with arbitrary linear adsorption and desorption rates. Our
22 benchmark problem demonstrates that predictions made with our proposed
23 SMM agree favorably with results from direct numerical simulations, which
24 resolve the full transport problem.

25 *Keywords:* Sorption Desorption, Upscaling, Spatial Markov Model

26 **1. Introduction**

27 Transport of chemical species through porous media can be complex rela-
28 tive to the flow through the medium due to the fact that constituents can sorb
29 and desorb to the solid matrix, thus slowing down their movement relative
30 to the flow. A common textbook approach to account for this is the inclu-
31 sion of a retardation coefficient in an advection dispersion equation (ADE)
32 [1]. This is only valid when (i) assumptions required to derive the ADE
33 for conservative transport hold and (ii) when one can assume that solute
34 in the fluid and solid phases is in an instantaneous well mixed equilibrium.
35 For complex porous media where geometries can give rise to heterogeneous
36 flows comprised of fast preferential flow channels as well as slower trapping
37 regions, such assumptions can be questionable. Even for conservative trans-
38 port, where there is no mass exchange between the fluid and the solid phase,
39 anomalous (non-Fickian) transport is known to occur, particularly at early
40 (preasymptotic) times [e.g. 2, 3]. The problem is further complicated with
41 the addition of potentially complex kinetic surface sorption and desorption
42 processes, which introduce their own set of potentially vastly different time
43 scales [4, 5].

44 In many instances, it is not of interest to explicitly describe and resolve
45 all details of transport at all scales, but rather model them effectively at
46 some scale of particular interest. Representing the transport of a solute in a
47 complex flow with a one-dimensional upscaled description can be dated back
48 to upscaling transport in cylindrical tubes by GI Taylor and Aris [6, 7]; this
49 was later generalized to more complex flow configurations using a variety of

50 related methods [e.g., 8, 9, 10]. In all cases, longitudinal transport can be
51 described with an effective one dimensional ADE with an enhanced Fick-
52 ian dispersion coefficient that reflects spreading due to subscale variations
53 in velocities. These models have been generalized to include a wide variety
54 of reactive processes including surface reactions and mixing processes [e.g.
55 11, 12, 13]. Dykaar & Kitanidis [12] calculated effective dispersion, velocity
56 and reaction rates in an idealized pore geometry by considering flow and
57 transport in a periodic channel with sinusoidal boundaries where solute can
58 react and degrade close to the boundaries, a process that is mathematically
59 similar to sorption. Levesque et al. [14] generalized Taylor dispersion to
60 systems that include adsorption and desorption to and from solid boundaries
61 in the flow domain and applied it to benchmark Poiseuille flows in planar
62 and cylindrical geometries, both in constant and periodic time varying flows.
63 In all cases effective velocities and dispersion coefficients can vary signifi-
64 cantly when compared to values obtained for a conservative solute. These
65 coefficients may also vary dynamically in time as recently shown in [15].

66 The above methods, in their original form, hinge on the assumption that
67 sufficient time has passed for the solute to sample the full variability of flow
68 velocities under displacements induced by diffusion. This is characterized
69 by the Taylor dispersion time scale $\tau_D = L^2/D$, where L is a characteristic
70 length scale and D the diffusion coefficient. At times smaller than this, the
71 aforementioned models are strictly speaking not valid. In the presence of re-
72 actions, the relative magnitude of reaction and transport characteristic time
73 scales becomes relevant to the applicability of continuum-scale models, such
74 as the standard advection-dispersion-reaction equation [e.g. 16, 17]. Depend-

75 ing on the nature of the problem at hand, this may or may not be important.
76 For example, many observations of so called anomalous or non-Fickian trans-
77 port [e.g. 18, 19, 20] are situations where all length and velocity scales of the
78 system have not yet been sampled and where the largest time scale might be
79 tremendously large relative to times of practical interest [e.g. 21, 22].

80 It is possible to relax this assumption and develop similar theories that are
81 valid at pre-asymptotic times [e.g. 23, 24, 25], but these still come with strong
82 assumptions that may or may not be met. A strong benefit of these models
83 is that they can help yield great physical insight into important processes at
84 small scales that dominate large scale behaviors. However, in some instances
85 the resulting models can be highly complex integro-differential equations with
86 strong memory effects, meaning that solving them can be as burdensome as
87 solving the full microscale problem [e.g. 26, 25].

88 The Spatial Markov model (SMM), first introduced by [27] provides an al-
89 ternative, relatively parsimonious approach that can be applied at preasymptotic
90 times, significantly earlier than Taylor dispersion [28]. The SMM falls
91 into the broad family of continuous time random walk (CTRW) models [29].
92 In the SMM, a solute plume is represented as a large number of infinitesimal
93 particles that transition through space and time. Most often, spatial incre-
94 ments are fixed and temporal increments are random, sampled from a mea-
95 sured transition time distribution. This is common to many CTRW models.
96 What sets the SMM apart is that successive temporal increments can be ex-
97 plicitly correlated, reflecting underlying persistence of fast particles to move
98 quickly and slow particles to move slowly, which is particularly important
99 in systems that are advection dominated [30]. The SMM has had success

100 in upscaling transport across a diverse set of transport settings, including
101 highly heterogeneous Darcy scale porous media [27, 31], fracture networks
102 [32], pore scale systems [33, 34, 30, 35], unsteady flows through porous media
103 [36], and a field scale application to a fractured aquifer [37]. The model has
104 recently been extended to incorporate nonlinear features such as mixing and
105 reactions [38, 39, 40]. In the above examples, the flows are typically either
106 highly heterogeneous with some random structure, or non-uniform, but with
107 a periodic unit cell, as commonly used in classical upscaling approaches such
108 as volume averaging [9, 41], the method of moments [8] or homogenization
109 [10, 42].

110 One of the criticisms of the SMM is that it can require extensive parame-
111 terization and the most common approach to date is to track Lagrangian par-
112 ticle statistics across two spatial increments, measuring particles transition
113 times across each and representing the correlation structure via a transition
114 matrix. Simplified forms have emerged which assume an idealized structure
115 to the transition matrix and have shown success [37, 43], but the assumed
116 structure may not be sufficiently general to be universal. More recently, an
117 approach was developed that takes successive breakthrough curves and infers
118 the transition matrix structure through an inverse modeling approach [44].
119 This was later applied to laboratory scale data of transport through zeo-
120 lite packed columns [45]. All of these approaches require information about
121 travel times across two spatial intervals. Within a domain composed of pe-
122 riodic cells, [40] developed an approach that only requires travel statistics
123 across one cell by parameterizing the model in terms of trajectories rather
124 than just travel times alone. Thus, with one high resolution simulation across

125 one cell (corresponding to one spatial increment in the SMM), they were able
126 to efficiently and rapidly predict large scale transport and mixing across much
127 greater extents, with the upscaled model running on the order of 1000 times
128 faster than a fully resolved one.

129 The work of [40] was only performed in the context of conservative trans-
130 port. Here we extend this approach to account for (linear) adsorption and
131 desorption processes. In particular, our goal is to only use trajectory statis-
132 tics from conservative non-sorbing transport across a single periodic cell to
133 predict larger scale transport of a solute that can adsorb and desorb to the
134 solid matrix with arbitrary adsorption and desorption rates; that is, we only
135 need one high resolution simulation across one periodic element with which to
136 ultimately predict a broad and extensive range of possible transport scenar-
137 ios across large scales. This extension to sorbing solutes opens the pathways
138 towards the application of this methods to a broad class of reactive trans-
139 port problems, such as contaminant transport in aquifers [46], as well as flow
140 through membranes and packed bed reactors [47, 48]. In this work we show-
141 case our modeling procedure by relying on a relatively simple flow geometry.
142 The simplicity of the geometry allows for a clear understanding of emergent
143 behaviors which can then be related to observations in more complex set-
144 tings. Thus, we regard it as an ideal starting point for our current extension
145 of the SMM. Moreover, a simple geometrical setting can provide critical in-
146 formation with which to parameterize pore network models and therefore
147 help bridge the gap between pore- and continuum-scale [e.g. 49].

148 2. Model system

149 2.1. Pore scale setting

150 Figure 1 displays the geometry used in this study, a converging-diverging
151 channel filled with fluid, whose solid boundaries are defined by

$$h(x) = \bar{h} + h' \sin\left(\frac{2\pi x}{L} - \frac{\pi}{2}\right), \quad (1)$$

152 where x is the horizontal coordinate, $h(x)$, \bar{h} and h' are related to the width
153 of the half-aperture (see Figure 1), and L is the length of a single cell. In
154 this study, to be consistent with previous ones [e.g. 40, 38], we will focus on
155 the specific values of $\bar{h} = L/4$ and $h' = 0.8\bar{h}$. This setting was first used
156 by [12] to upscale effective reaction rates in porous media using the method
157 of moments. While this geometry is very simple, the emergent flow displays
158 some of the complex features pertinent to understanding flow and transport
159 in porous media, including a fast preferential flow path and stagnant trapping
160 areas, which are known to strongly impact transport in real porous media
161 [e.g. 50]. This, and very similar geometries, have received extensive atten-
162 tion in the literature. For example, [51, 52] and [53, 30] studied the effects
163 of inertia on flow and transport respectively. Similarly, others have looked
164 at how geometry impacts asymptotic [54, 55] and pre-asymptotic transport
165 [56, 57], as well as the role of turbulence on large scale dispersion [23]. One of
166 the reasons we choose this geometry is that under the assumption of Stokes
167 flow, i.e. Reynolds number less than $O(1)$, a semi-analytical solution exists
168 [58, 12]. The solution uses a perturbation method to solve the biharmonic
169 equation, which governs the streamline structure. Details of the solution, as

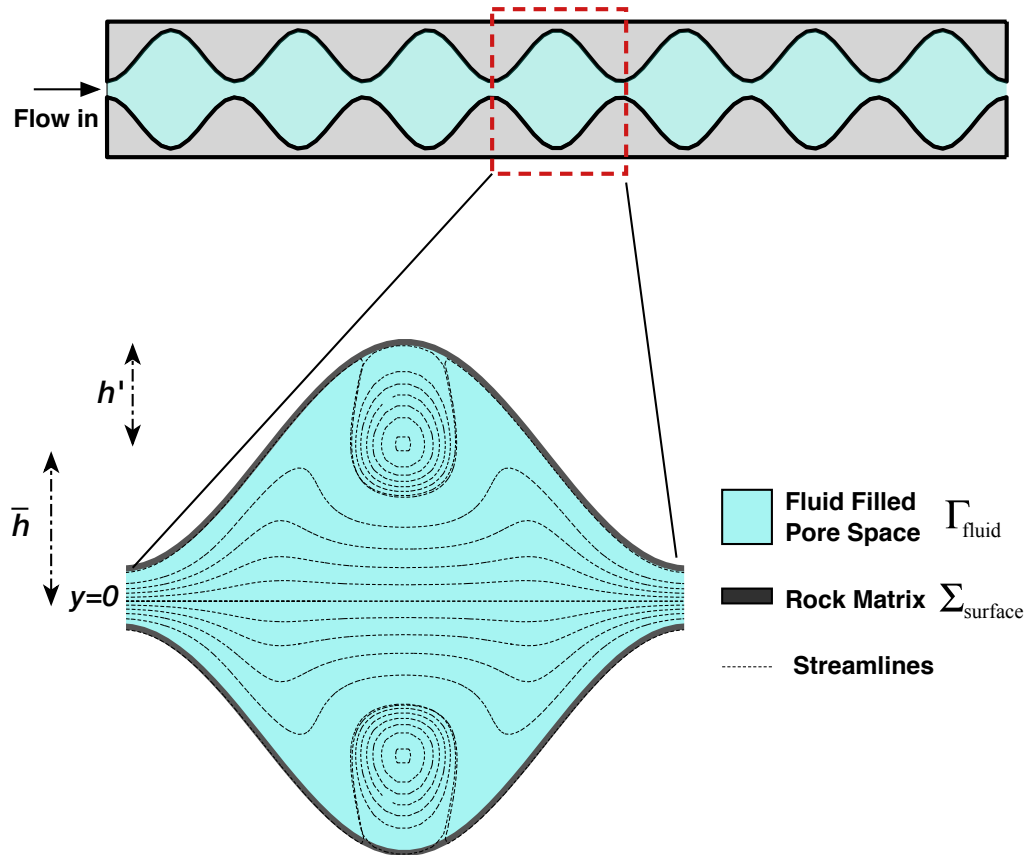


Figure 1: A schematic of the flow domain and the unit pore cell used in this study.

170 well as its validation are available in various papers [58, 12, 59, 55] and so are
 171 not elaborated on here. The geometry defined above is chosen because of the
 172 interesting flow patterns, including the emergence of a recirculation region
 173 and a fast central preferential flow channel. While the geometry is highly
 174 idealized, these specific features mimic features of interest in real porous me-
 175 dia, making this model potentially appealing. Due to the natural symmetry
 176 of the system throughout this entire work we only ever simulate the top half
 177 of the domain ($y > 0$).

178 *2.2. Simulation of transport at the microscale*

179 Solute transport with sorption and desorption is modeled by [60, 15]

$$\begin{aligned} \frac{\partial C(\mathbf{x}, t)}{\partial t} + \nabla \cdot [\mathbf{u}(\mathbf{x})C(\mathbf{x}, t)] &= \nabla \cdot [D\nabla C(\mathbf{x}, t)] & \forall \mathbf{x} \in \Gamma_{fluid} \\ \frac{\partial S(\mathbf{x}, t)}{\partial t} &= -\lambda S(\mathbf{x}, t) + \alpha C(\mathbf{x}, t) = D \frac{\partial C(\mathbf{x}, t)}{\partial n} & \forall \mathbf{x} \in \Sigma_{surface} \end{aligned} \quad (2)$$

180 where $C(\mathbf{x}, t)$ [ML^{-3}] is the concentration of the solute in the fluid, $\mathbf{u}(\mathbf{x})$ is
 181 the velocity in the fluid phase, D [L^2T^{-1}] is the molecular diffusion coeffi-
 182 cient, taken to be constant in the fluid, $S(\mathbf{x}, t)$ [ML^{-2}] is the concentration
 183 on the surface, λ [T^{-1}] is the rate of desorption, α [LT^{-1}] is the rate of
 184 adsorption and n is the unit normal to the boundary. Note that the first
 185 equation in (2) describes transport in the main channel, which is governed
 186 by the advection diffusion equation. The second equation is the boundary
 187 condition, describing exchange between the fluid and solid phase: the rate
 188 of change of surface concentration is given by the rate at which solute con-
 189 centration attaches to the boundary (αC) minus the rate which solid phase
 190 concentration is detaching (λS); for mass balance reasons this must be equal

191 to the diffusive flux of solute concentration at the boundary ($D \frac{\partial C(\mathbf{x}, t)}{\partial n}$). In
 192 all cases we consider an initial condition of an instantaneous line source, flux
 193 weighted along the pore throat, i.e. $C(\mathbf{x}, t = 0) \propto \mathbf{u}(\mathbf{x})\delta(x)$. This choice of
 194 initial condition is common as it is believed to mimic real experiments [e.g.
 195 61, 62] and also represents the asymptotic distribution to which Lagrangian
 196 particles are expected to converge [e.g. 63, 64, 65]

197 To solve this system we implement a numerical Lagrangian particle based
 198 random walk method [66], where the solute plume is discretized into a finite
 199 number of N particles. We incorporate the sorption-desorption boundaries
 200 following the work of [67]. During each step each particle is moved according
 201 to Langevin equation

$$\begin{aligned}
 x_i^{n+1} &= x_i^n + u_i \Delta t + \xi_i \sqrt{2D\Delta t} \\
 y_i^{n+1} &= y_i^n + v_i \Delta t + \eta_i \sqrt{2D\Delta t} \quad i = 1, \dots, N, \\
 t_i^{n+1} &= t_i^n + \Delta t + \tau_i
 \end{aligned} \tag{3}$$

202 where x_i^n and y_i^n are the horizontal and vertical position of particle i re-
 203 spectively at simulation step n , u_i and v_i are the x and y components of
 204 the velocity respectively, ξ and η are independent and identically distributed
 205 (iid) Gaussian variables with zero mean and unit variance, Δt is a fixed time
 206 step, t_i^n is the time for particle i at simulation step n , and τ_i is a random
 207 waiting time

$$\tau_i = \begin{cases} T_i : P > U_i \\ 0 : P \leq U_i \end{cases}, \tag{4}$$

208 where the T_i are iid exponential, with density $\psi(\tau) = \lambda \exp[-\lambda\tau]$, P is the
 209 probability of sorption and U_i are iid $U(0, 1)$ (uniformly distributed between 0
 210 and 1). The solid boundaries in the domain are modeled as elastic reflection
 211 boundaries. Any time a particle reflects off a solid boundary it either sorbs
 212 with probability P , resulting in selecting τ randomly from $\psi(\tau)$, or does not
 213 sorb, resulting in $\tau = 0$. To leading order, this probability can be computed
 214 as

$$P = \alpha \sqrt{\frac{\pi \Delta t}{D}}. \quad (5)$$

215 For further details on this as well as higher order approximations please see
 216 [67]. This number P is compared to a random number U , drawn from a
 217 standard uniform distribution. If $U \geq P$ no sorption occurs and if $U < P$
 218 the particle sorbs.

219 Our choice of solving this system using this Lagrangian random walk
 220 method is based on the following: (i) it naturally aligns with building an
 221 SMM, which relies on Lagrangian statistics, (ii) for a periodic system like
 222 this one, it is possible to simulate very extensive domains as a particle's
 223 velocity at any given time depends only on its local position relative to the
 224 periodic cell, meaning that we do not need a prohibitively large Eulerian
 225 mesh and (iii) for a sufficiently smooth velocity field, such as this one, it is
 226 known not to suffer from numerical dispersion, which could be problematic
 227 since diffusion and adsorption processes are closely linked. For all of the
 228 results that we present in this paper we used one million particles and a time
 229 step of $\Delta t = 10^{-3}$, consistent with previous experience in the same domain
 230 [55].

231 *2.3. Dimensionless numbers*

232 The system described in section 2.2 is characterized by the following di-
 233 mensionless numbers

$$Re = \frac{\bar{h}\bar{u}}{\nu} \quad Pe = \frac{\bar{h}\bar{u}}{D} \quad Da_a = \frac{\bar{h}\alpha\sqrt{\pi}}{D} \quad Da_d = \frac{\bar{h}^2\lambda}{D}. \quad (6)$$

234 \bar{u} is the mean velocity and ν is the viscosity of the fluid. Re is the Reynolds
 235 number, which we have already assumed to be small $Re < O(1)$ in using the
 236 prescribed flow field; Pe is the Péclet number, which reflects the competition
 237 between advection and diffusion processes and typically lies in the range
 238 $0.1 < Pe < 10^3$ [12]. We will focus on the higher range of these values,
 239 as it is known that advection-dominated systems are more likely to violate
 240 assumptions inherent to Taylor dispersion and classical advection-disperison
 241 upscaling. Da_a and Da_d are adsorptive and desorptive Damköhler numbers,
 242 which respectively compare the time scales associated with adsorptive and
 243 desorptive processes to diffusive ones. In a batch system, large values of these
 244 would correspond to systems close to equilibrium between surface and fluid
 245 concentrations. In the following any reported dimensionless parameters are
 246 obtained by setting $\bar{u} = 1$, $2\bar{h} = 1$ (in arbitrary units) and tuning D , α and
 247 λ to obtain specified values of Pe , Da_a and Da_d .

248 *2.4. Inputs for Spatial Markov Model - trajectories, travel times and number*
 249 *of hits*

250 Here we define the inputs that must be obtained from the microscale
 251 domain in order to build the macroscale effective SMM, described in the
 252 following section. In all cases we obtain these inputs by running a random

253 walk with a flux weighted pulse initial condition at the throat of a pore (see
 254 figure 1) and simulate transport across one periodic unit cell. This calibration
 255 simulation is for a conservative random walk that does not include sorption.
 256 The periodic unit cell corresponds to the blown up region in figure 1. Sund
 257 et al’s [40] SMM is different from others in that it samples trajectories rather
 258 than travel times. These trajectories are obtained by simulating transport
 259 across a single unit cell, using

$$\begin{aligned}
 x_i^{n+1} &= x_i^n + u_i \Delta t + \xi_i \sqrt{2D\Delta t} \\
 y_i^{n+1} &= y_i^n + v_i \Delta t + \eta_i \sqrt{2D\Delta t}
 \end{aligned}
 \quad i = 1, \dots, N . \quad (7)$$

260 This is a standard random walk framework (note these equations are the
 261 same as (3), but without the random waiting times associated with model-
 262 ing sorption). Using this we store specific information about each particle’s
 263 trajectory. In Sund’s approach each trajectory is defined by three param-
 264 eters: (i) its vertical position at the inlet of the periodic element y_{in} , (ii) the
 265 time, T , it takes to travel from the inlet to the outlet and (iii) its vertical
 266 position at the outlet when it leaves the periodic element y_{out} . In addition
 267 to these three inputs, our method will account for adsorption-desorption by
 268 storing one additional piece of information (iv) N_{hits} , the number of times
 269 a particle strikes a solid boundary when crossing a single cell. We propose
 270 that by running one high resolution simulation of conservative transport over
 271 one periodic element, we can obtain all of the required information needed
 272 to upscale and describe transport with adsorption and desorption efficiently
 273 over much larger scales. However, it must be noted that for each different

274 value of Pe , a different calibration simulation is required.

275 2.5. Effective transport model - The Spatial Markov Model

276 Here we propose an SMM, which is an effective upscaled transport model
277 that describes transport in one dimension aligned with the direction of flow.
278 The SMM is a time domain random walk model and again the solute is
279 represented by discrete particles, whose motion in time and space is governed
280 by:

$$\begin{aligned}\tilde{x}_i^{k+1} &= \tilde{x}_i^k + L \\ \tilde{t}_i^{k+1} &= \tilde{t}_i^k + T_i^k + \sum_{j=1}^{N_{hits}^k} \tau_j.\end{aligned}\tag{8}$$

281 Tildes refer to upscaled quantities. \tilde{x}_i^k is the horizontal location of particle
282 i at the beginning of step k , \tilde{t}_i^k is the time associated with particle i at the
283 beginning of step k , N_{hits}^k is the number of times the sampled trajectory
284 strikes the boundary during step k . During each step a particle transitions
285 a constant longitudinal distance L , the length of our periodic cell, and it
286 does so in a random time T , which is sampled from a measured travel time
287 distribution, the discrete distribution obtained from the single pore calibra-
288 tion simulation in (7). T reflects the range of velocities that particles sample
289 in traversing the unit cell. The feature that makes the SMM unique rel-
290 ative to other random walk models is that successive temporal increments
291 are not independent of one another. Correlation arises when a particle that
292 traverses one periodic unit quickly is also likely to traverse the next one

293 quickly and likewise for a slow one. In the absence of diffusion, particles per-
 294 sist on the same streamline always and so successive jumps would have the
 295 same transition time. Due to diffusion, particles can leave streamlines and
 296 sample various flow streamlines. However, when advective effects are strong
 297 relative to diffusive ones, memory effects persist and must be accounted for
 298 through correlation. In most applications, correlations are applied using a
 299 transition matrix [27]. We apply here instead the trajectory based approach
 300 recently proposed in [40], because the trajectory based method can account
 301 for the number of times each trajectory interacts with the boundary in a way
 302 that the original transition matrix approach cannot. This approach naturally
 303 provides a framework that more readily characterizes interactions of particles
 304 with the reactive boundary, using the information stored as inputs for the
 305 SMM described in §2.4. It should be noted that the periodic nature of the
 306 domain is important in accomplishing this, although some other recent stud-
 307 ies suggest that trajectory based methods may also work for heterogeneous
 308 systems characterized by a stationary heterogeneity distribution [68, 69].

309 In this implementation of the model, each step of length L is associated
 310 with a specific particle trajectory. We summarize our algorithm in the fol-
 311 lowing steps:

- 312 1. Each particle starts with a given y_{in} reflecting the desired initial condi-
 313 tion. This sets a specific trajectory that has an associated travel time,
 314 which is used as the time increment T_i^k in (8), and an assigned number
 315 of hits N_{hits}^k .
- 316 2. Adsorption is accounted for by the term $\sum_{j=1}^{N_{hits}^k} \tau_j$, where each strike
 317 with the boundary adds a possible waiting time, which is sampled from

318 the same distribution $\psi(\tau)$ as used in (3) with probability P from (5).
319 3. The model then samples the next trajectory randomly, using y_{out} as a
320 conditioning criterion for picking the next trajectory by making sure
321 that its y_{in} is close to the previous y_{out} . This is done by discretizing
322 the inlet into N_{bins} equi-sized bins (we used cases with $N_{bins} = 10$,
323 100 and 1000 in this study with no notable difference in results). A
324 particle's vertical y location determines which bin it is in. Thus y_{out}^k
325 determines the bin from which the next trajectory is sampled. A tra-
326 jectory with y_{in}^{k+1} is randomly and uniformly sampled from the same
327 bin that y_{out}^k ends in. This binning procedure ensures correlation effects
328 are accurately imposed.

329 *2.6. Observables to test model*

330 We will test the proposed SMM by comparing its ability to predict down-
331 stream transport as measured by breakthrough curves (BTCs) measured at
332 multiple downstream locations. These are $x = 5L, 10L, 25L$ and $50L$. Test-
333 ing the upscaled model against BTCs at multiple downstream locations pro-
334 vides a more robust test of the model compared with focusing on only one
335 location; sometimes a model can match a single BTC due to overparameter-
336 ization, but when the same model can consistently match observations over
337 multiple scales, it suggests that the underlying physics is being more faith-
338 fully captured. Thus, to produce benchmark data against which to test the
339 SMM, we run a series of high resolution random walk simulations using the
340 fully resolved transport equations (3) that account for advection, diffusion,
341 adsorption and desorption. In all cases we use a flux weighted pulse ini-
342 tial condition and run single realization simulations with $N = 10^6$ particles.

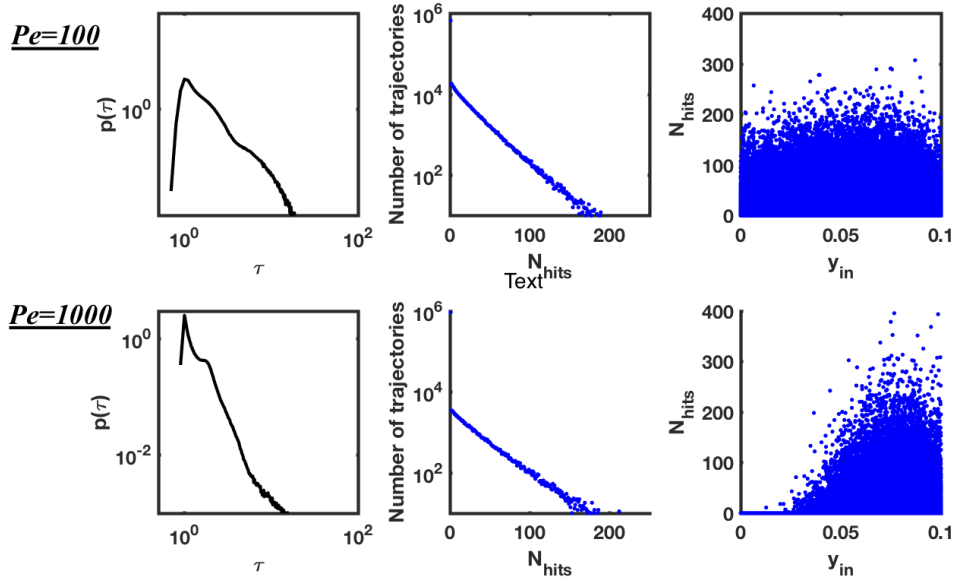


Figure 2: (Left) Travel Times Distributions across single periodic elements (Middle); Frequency scatter plot of number of times each trajectory hit the boundary; (Right) Scatter plot for each simulated particle's starting y_{in} vs the number of times a particle hits the boundary during one travel time. The top row shows results for $Pe = 100$ and the bottom row for $Pe = 1000$.

343 These results are the reference solution against which the upscaled model is
 344 tested.

345 **3. Results**

346 *3.1. Travel Time Distributions and Number of Hits*

347 Figure 2 displays the empirical travel time distributions, measured from
 348 simulations, across a single periodic element for two cases, $Pe = 100$ and
 349 $Pe = 1000$. The data used to plot these travel time distributions is from
 350 where temporal increments are sampled. These two Péclet numbers are cho-
 351 sen because, in the case of purely conservative transport, it has been shown

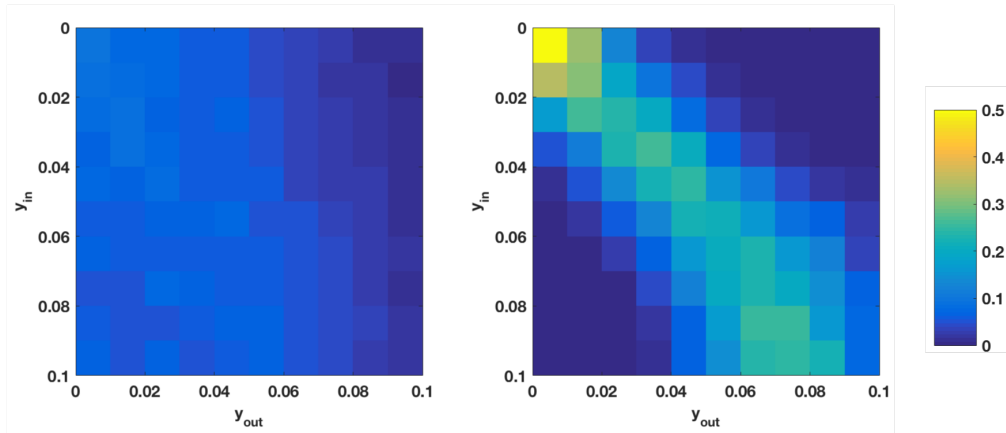


Figure 3: Transition probabilities of y_{out} given y_{in} for $Pe = 100$ (left) and $Pe = 1000$ (right). In this figure y_{in} and y_{out} are discretized into 10 bins of equal size.

352 that for $Pe = 100$ incorporating correlation effects is unimportant, while for
 353 $Pe = 1000$ it is [30]. These distributions were obtained by creating a his-
 354 togram of arrival times and normalizing. The bin size of the histogram grew
 355 logarithmically with larger τ .

356 Also shown are the number of times a particle (trajectory) strikes the
 357 boundary during a given transition across a single cell. Most notably, for
 358 both Péclet numbers the vast majority (approximately 99%) of trajectories
 359 never actually strike the boundary and pass through the pore with no possi-
 360 bility of adsorption taking place. However, some trajectories can strike the
 361 boundary anywhere up to 200 times, meaning that the likelihood of adsorp-
 362 tion can be significant depending on the adsorption rate, or the probability
 363 of attachment P . For the lower Péclet number case more trajectories strike
 364 the boundary than in the $Pe = 1000$ case, which intuitively makes sense
 365 given that the surface reaction is diffusion-driven. The expected delay for a
 366 reactive particle that strikes the boundary N_{hits} times is $\langle\tau\rangle = \frac{N_{hits}P}{\lambda}$, where

367 the angled brackets denote the expected value.

368 Finally, figure 2 shows a scatter plot of each simulated trajectory’s start-
369 ing location at the inlet against the number of interactions with the boundary.
370 This figure clearly highlights that for the $Pe = 1000$ case a particle has to
371 start near the boundary in order to have any chance of interacting with it.
372 A particle that starts on the centerline $y = 0$ has nearly zero likelihood of
373 interacting with the boundary and thus adsorbing. For the $Pe = 100$ the
374 number of hits per trajectory is relatively independent of y_{in} . This suggests
375 that accounting for correlation effects (i.e. knowing a particle’s starting loca-
376 tion as it transitions through each pore) may be less important for $Pe = 100$
377 than for $Pe = 1000$, as found in the conservative case [30].

378 Figure 3 displays the discrete transition probabilities that a particle has
379 for a y_{out} given a particular y_{in} , which is a measure of correlation. Note
380 that this figure is an approximation of the copula density function defining
381 correlation between travel times in consecutive steps [70]. As has been seen
382 in previous studies for $Pe = 100$, this matrix is relatively uniform, while
383 there is a stronger diagonal dominance for the $Pe = 1000$ case reflecting the
384 fact that correlation effects become stronger as Péclet number increases [30].

385 3.2. Comparison between DNS and SMM predicted breakthrough curves

386 3.2.1. Limit of no sorption ($P = 0$)

387 To begin, we demonstrate the proposed SMM’s ability to upscale trans-
388 port in the absence of any sorption at all. Plots comparing breakthrough
389 curves at multiple downstream locations measured by DNS and predicted
390 with the SMM are shown in Figure 4. As in previous studies, the agreement
391 is excellent demonstrating the veracity of our proposed approach.

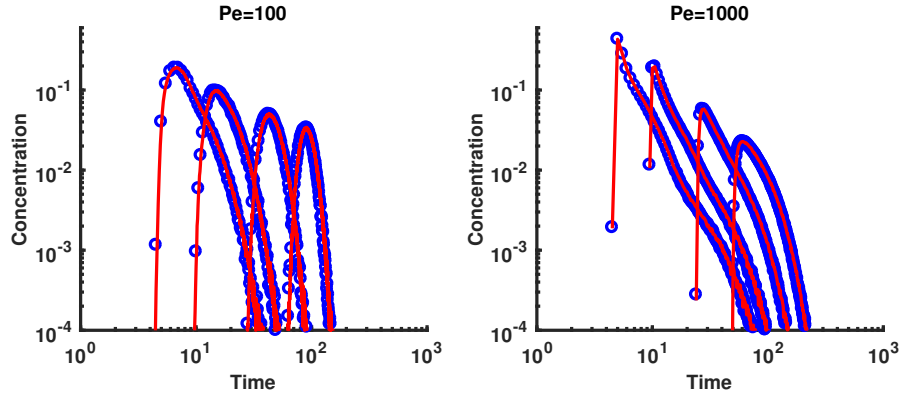


Figure 4: Breakthrough Curves for $Pe = 100$ (left) and $Pe = 1000$ (right) at distances of $5L$, $10L$, $25L$ and $50L$ with no sorption at all. Blue dots are DNS results and black lines are SMM predictions.

392 3.3. Limit of unit probability

393 Next we focus on another limiting case, where the probability of sorption
 394 each time a particle strikes the boundary is unity ($P = 1$), meaning that
 395 every strike results in an adsorption event. While this may not be an en-
 396 tirely physical condition, by considering this extreme case we are testing our
 397 proposed procedure across a wide range of possible Da_a . For $Pe = 100$ and
 398 $Pe = 1000$ the respective values are $Da_a = 316$ and $Da_a = 10^3$. The consid-
 399 ered values of $\lambda = 0.1$ and 1 correspond to $Da_d = 10, 10^2$ and $Da_d = 10^2, 10^3$
 400 respectively.

401 Results comparing DNS measured breakthrough curves as well as SMM
 402 predicted ones are shown in figure 5. Additionally, for context and to ex-
 403 plicitly demonstrate the role of sorption, breakthrough curves for the case of
 404 zero sorption, as discussed in the previous section, are also included. Again,
 405 the agreement between DNS and SMM is excellent, with the SMM capturing
 406 all essential features displayed by the fully resolved simulations.

407 For the $Pe = 100$ case the rising limb of the two earlier breakthrough
408 curves is similar for the cases with and without sorption. This corresponds
409 to fast moving particles following trajectories that never interact with the
410 boundary. The late time behavior and the further downstream breakthrough
411 curves are very distinct with a strong separation between the case with and
412 without sorption, reflecting strong delays due to sorption. For the $Pe = 1000$
413 case more particles persist at moving quickly and do not interact with the
414 boundary; thus the early arrivals are similar between cases with and without
415 sorption. Again, at late times there is a deviation between the cases with
416 strong delays in the tails emerging for the cases with sorption.

417 3.4. Intermediate sorption

418 Results corresponding to a sorbing probability that is one order of mag-
419 nitude smaller than in the previous section, $P = 0.1$, are shown in figure 6,
420 which correspond to $Da_a = 31.6$ and 100 . The results demonstrate that the
421 SMM provides reliable results across the parameter space.

422 The resulting breakthrough curves reflect very similar behavior to the
423 previous case; however the tails are not as delayed, reflecting the fact that
424 only 10% of particles that sorbed in the $P = 1$ case actually do so here. For
425 the $Pe = 1000$ and $Da_d = 1000$ case ($\lambda = 1$, Figure 6 top right), it is visually
426 next to impossible to see differences at late times, while for the longer waiting
427 time $Da_d = 100$ ($\lambda = 0.1$, Figure 6 bottom right) a more distinct delayed
428 tailing behavior emerges for the cases with sorption. Note that breakthrough
429 curves obtained with $P = 0.1, \lambda = 0.1$ (bottom row in figure 5) are identical
430 to the ones for $P = 1, \lambda = 1$ case (top row in figure 4) because their expected
431 delay times are equivalent. This is because, on average, multiplying both P

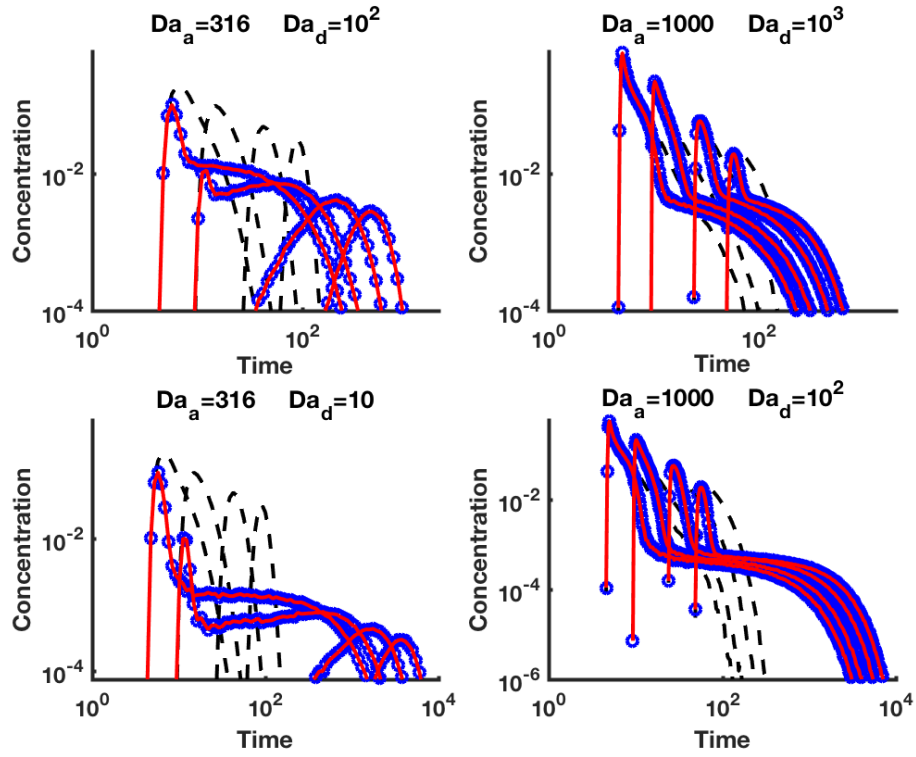


Figure 5: Breakthrough Curves for $Pe = 100$ (left) and $Pe = 1000$ (right) at distances of $5L$, $10L$, $25L$ and $50L$ with sorption given by $P = 1$. Blue dots are DNS results and red lines are SMM predictions. Black dash-dot lines are BTCs for the case without sorption.

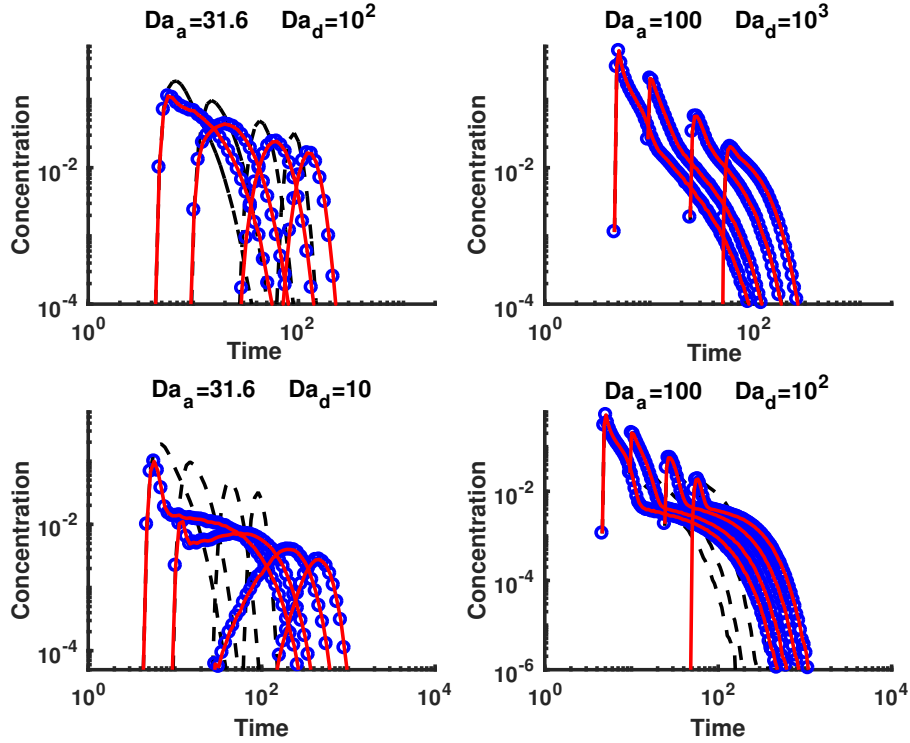


Figure 6: Breakthrough Curves for $Pe = 100$ (left) and $Pe = 1000$ (right) at distances of $5L$, $10L$, $25L$ and $50L$ with sorption given by $P = 0.1$. Blue dots are DNS results and red lines are SMM predictions. Black dash-dot lines are BTCs for the case without sorption.

432 and λ by a constant has no effect on average travel times.

433 3.5. The role of correlation

434 In this section, we test how important including correlation in the SMM is
 435 for accurately predicting downstream reactive transport behavior. To do so,
 436 an uncorrelated one-dimensional time domain random walk (TDRW) model
 437 is built by simply sampling random trajectories without considering the inlet
 438 and outlet locations, which are the quantities by which we enforce correlation
 439 in our model. The trajectories are sampled uniformly from the calibration

440 simulation data.

441 Figure 7 shows the comparisons for all parameter choices considered so
442 far, but focusing only the furthest downstream BTC ($x = 50L$). As expected,
443 the importance of correlation effects is stronger for the $Pe = 1000$ cases than
444 for $Pe = 100$. However, even for $Pe = 100$ distinguishable errors are visible
445 where successive travel times are sampled independently. This suggests that,
446 while correlation effects are seemingly unimportant for the $Pe = 100$ case for
447 conservative transport [30], as sorption at the boundary occurs, correlation
448 begins to play some role, similar to what has been observed for reactions [38].

449 Notably, when correlation is not accounted for, predicted breakthrough
450 curves fail to capture the full rising limbs and also display greater delays than
451 the actual measured ones. This reflects the fact that too many particles are
452 interacting with the boundary. The uncorrelated model cannot account for
453 the fact that fast particles have a tendency to persist at staying fast, as well
454 as the fact that the fastest particles have virtually no probability of getting
455 sorbed, as shown in figure 2.

456 While well known that correlation plays an ever more important role as
457 the Péclet number of a system increases, the effect of boundary reactions on
458 the importance of correlations between successive jumps has not been previ-
459 ously explored. Figure 8 quantifies this effect based on the approximation of
460 particle arrival times. More specifically, we consider the recovered mass at
461 time t

$$M(t) = \int_0^t C(x = 50L, t') dt' \quad (9)$$

462 which is the cumulative distribution function of solute arrival times at $x =$
463 $50L$. We compute the mean absolute error ($MAE = \sum_{i=1}^{N_t} |M_{DNS}(t_i) -$

464 $M_{simulated}(t_i)$) between the results obtained via DNS and the upscaled sim-
 465 ulation with uncorrelated steps at location $50L$. Our results, in agreement
 466 with previous studies, show that the uncorrelated model can yield accurate
 467 arrival times of a nonreactive solute ($Da_a = 0$) for $Pe = 100$ as the MAE
 468 attains a value of $\sim 5 \times 10^{-5}$. The occurrence of adsorption induces an in-
 469 crease of the MAE by approximately two orders of magnitude, irrespective of
 470 the probability with which reaction occurs. This is likely because only slower
 471 particles ever interact with the boundary and, while weak, some correlation
 472 does occur. This does not mean that the model is not sensitive to P ; indeed
 473 it must be since larger values of P result in larger delays. It is only saying
 474 that correlation effects may be more important to include in the upscaled
 475 model when sorption occurs. Note that when correlation is included the
 476 MAE is approximately constant for all adsorption probabilities (including
 477 the conservative case, $P = 0$) and attains a value of approximately 10^{-5} (not
 478 shown).

479 Additionally, to provide another basis for comparison, Table 1 shows the
 480 arrival times when 1%, 50% and 99% of the mass has arrived for all of the
 481 cases shown in Figure 7. We show the dimensionless time for DNS and the
 482 relative difference R_Δ between DNS and the two models, computed as

$$R_\Delta(MOD) = \frac{t_{pc}(MOD) - t_{pc}(DNS)}{t_{pc}(DNS)} \quad (10)$$

483 where MOD stands for UNC (uncorrelated TDRW) or SMM and t_{pc} indi-
 484 cates the time corresponding to arrivals of percentile pc of total mass (i.e.,
 485 pc equals 1%, 50% and 99% here). These results clearly and quantitatively
 486 highlight the good agreement between the DNS and SMM as well as the afore-

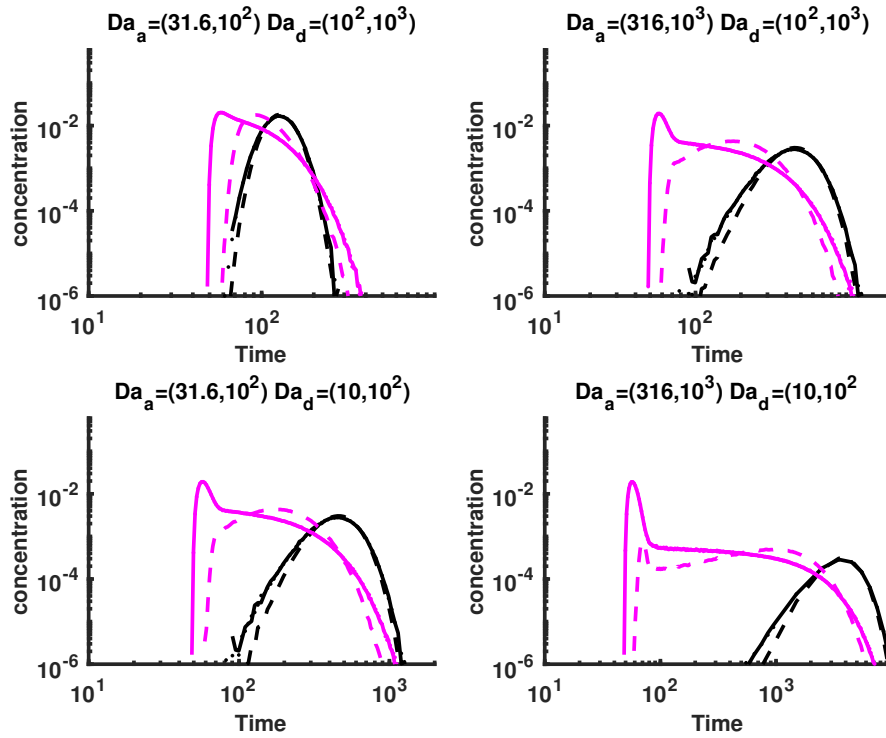


Figure 7: Breakthrough curves at a distance of $50L$ for $Pe = 100$ (black) and $Pe = 1000$ (magenta). Solid lines are the SMM with correlation effects included, while dashed lines do not include correlation effects. Dots are results from the DNS simulations (note that these are hard to see as they coincide so closely with the SMM results). Damköhler numbers in parentheses are for $Pe = 100$ and 1000 respectively.

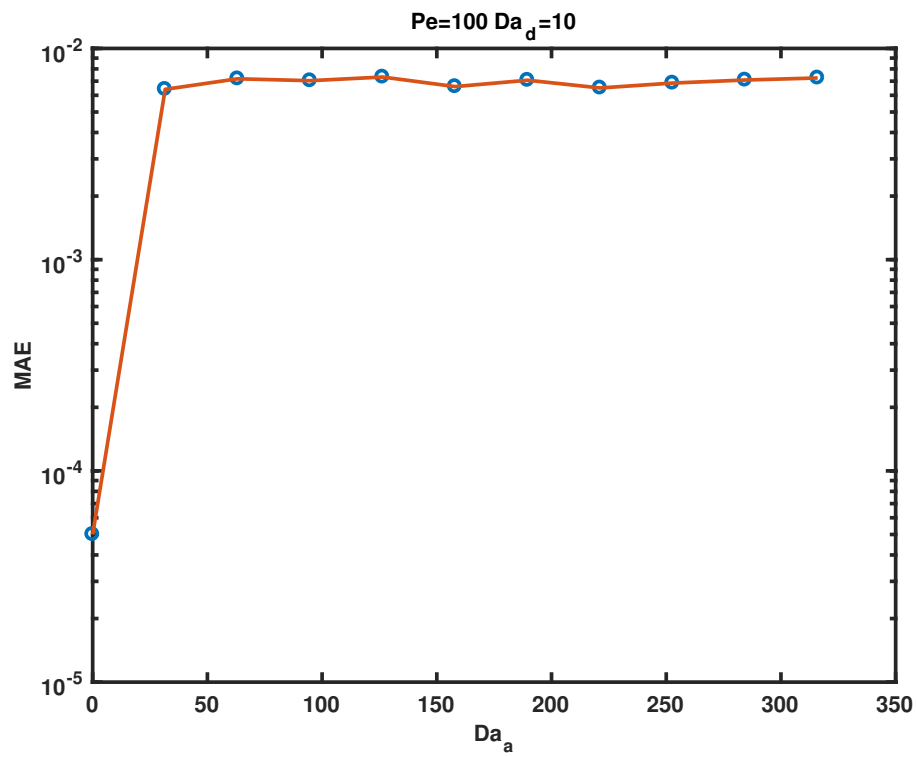


Figure 8: Mean absolute error (MAE) between recovered mass simulated by direct numerical simulation and uncorrelated simulations at $50L$, for $Pe = 100$ and $Da_d = 10$ as a function of Da_a .

487 mentioned discrepancies between the DNS and uncorrelated TDRW model.
488 Differences between DNS and SMM are always within 1%, showing the ro-
489 bustness of the method. On the other hand, when correlations are neglected,
490 the errors increase sharply with Pe , i.e. relative differences between uncor-
491 related model and DNS are up to 10-15% for $Pe = 100$ and up to 90% for
492 $Pe = 1000$. In general, the uncorrelated TDRW overestimates early arrivals
493 and underestimates late arrivals. Correlation effects also appear to have dif-
494 ferent influence depending on Da_a and Da_d . These differences emerge in
495 the 1% and 50% arrival times (early arrivals and median time), although
496 with relatively smaller variations than the ones observed for Pe . For early
497 arrivals and median time, the uncorrelated model errors tend to increase for
498 increasing Da_a and decrease with increasing Da_d , i.e. the error may change
499 up to a factor 2 when the two Damköhler numbers change by one order of
500 magnitude.

Table 1: Arrival times for 1, 50, and 99% of the solute plume to cross $50L$ in the DNS and relative difference R_Δ related to the upscaled SMM, and uncorrelated TRDW (UNC). Cases correspond to different combinations of adsorptive and desorptive Damköhler numbers.

$Pe = 100$									
Case	1% Arrival Time			50% Arrival Time			99% Arrival time		
	DNS	$R_\Delta(SMM)$	$R_\Delta(UNC)$	DNS	$R_\Delta(SMM)$	$R_\Delta(UNC)$	DNS	$R_\Delta(SMM)$	$R_\Delta(UNC)$
$Da_a = 31.6, Da_d = 10$	208.5	0.58%	11.68%	478.5	0.31%	0.71%	888.4	-0.14%	-3.82%
$Da_a = 31.6, Da_d = 100$	85.9	0.23%	5.34%	130.9	0.15%	0.46%	198.9	-0.30%	-2.72%
$Da_a = 316, Da_d = 10$	1416.8	0.77%	15.09%	3953.1	0.40%	0.73%	7800.7	0.21%	0.73%
$Da_a = 316, Da_d = 100$	208.6	0.48%	11.78%	478.7	0.21%	0.73%	886.6	0.00%	-3.46%
$Pe = 1000$									
$Da_a = 100, Da_d = 100$	52.3	0.19%	42.94%	139.8	0.50%	52.46%	635.1	0.60%	-13.35%
$Da_a = 100, Da_d = 1000$	52.3	0.19%	34.73%	84.4	0.36%	23.26%	219.7	0.59%	-10.18%
$Da_a = 1000, Da_d = 100$	52.3	0.00%	76.77%	675.2	1.13%	89.84%	4911.7	1.09%	-12.92%
$Da_a = 1000, Da_d = 1000$	52.3	0.00%	42.83%	139.9	0.43%	52.60%	635.1	0.60%	-13.35%

501 4. Discussion and conclusions

502 We have extended the Spatial Markov Model for periodic flow domains
503 proposed in [40] to account for linear adsorption to and desorption from solid
504 boundaries. In particular, we have built the framework based on a trajectory
505 based SMM, where high resolution trajectories simulated by an advective-
506 diffusive random walk over a single periodic flow element are stitched to-
507 gether sequentially to predict transport over much larger scales. In this
508 novel approach we merely store one additional piece of information about
509 each trajectory, that is the number of times that it strikes a solid boundary.
510 This information reflects the solute flux close to the boundary surface that
511 corresponds to the adsorption reaction rate. Coupling this with a proba-
512 bilistic representation of sorption [67], we can effectively upscale transport
513 to represent arbitrary adsorption and desorption rates. Thus from a sin-
514 gle high resolution random walk simulation of conservative transport across
515 one periodic element we can model an extremely diverse range of adsorp-
516 tion/desorption behaviors without the need to run further high resolution,
517 computationally intensive, small scale simulations for each desired case. Of
518 course this current application is strictly restricted to the example of an ide-
519 alized periodic setting and it remains to be shown how generalizable it is to
520 more complex and realistic settings.

521 As in previous studies of conservative transport, the need for the upscaled
522 model to account for correlation between successive jumps depends on the
523 Péclet number of the system, with correlation being more important as ad-
524 vection begins to dominate more and more. Similarly, it appears that the
525 Damköhler numbers play a role in determining this, meaning that merely

526 delineating regions where correlation is important or unimportant for con-
527 servative transport does not provide a sufficient condition for the case when
528 reaction occurs. This is particularly relevant for the accurate representation
529 of early and late particle arrivals with the upscaled model, because these are
530 most sensitive to correlation effects (fast particles tend to persist as fast and
531 slow as slow). For the conditions explored, we have numerically verified that
532 the correlation between subsequent travel times plays a relevant role across
533 the full range of investigated adsorption rates. As expected, the relevance
534 of correlation is sharply influenced by Pe , but also increases with Da_a (fast
535 adsorption) and decreases with Da_d (fast desorption). This trend is particu-
536 larly striking for early arrivals, which could be of practical relevance, e.g., in
537 assessment of membranes life-cycle or of risk with contaminant breakthrough
538 in aquifers. Notably, our approach conserves the same accuracy with respect
539 to fully resolved simulations for both conservative and reactive transport.

540 Our model can accurately upscale kinetic sorption and desorption pro-
541 cesses, i.e. it does not assume equilibrium between sorbed and dissolved
542 solute mass, as would be the case if modeling adsorption/desorption with
543 a retardation coefficient. We emphasize that the traditional use of a retar-
544 dation factor to account for the delays in transport induced by adsorption
545 and desorption will not work to reproduce the cases that we simulate here.
546 The main effect of a retardation coefficient would simply be a rescaling in
547 time of a conservative concentration profile or breakthrough curve. However,
548 the breakthrough curves obtained in this study, in many cases, have a fun-
549 damentally different shape from those without adsorption and desorption.
550 The use of a retardation coefficient assumes an instantaneous equilibrium

551 between mobile and immobile parts of the domain and clearly that is not the
552 case here, particularly for the higher Péclet number case. The persistence
553 of correlation effects is very much inline with the fact that highly mobile
554 particles traveling on fast trajectories have virtually no interaction with the
555 boundaries while slower ones can have many, reflecting a lack of equilibrium.
556 As with upscaling of other transport processes, at late times as systems begin
557 to homogenize (i.e. greater than Taylor time scales) conditions for such an
558 equilibrium can arise, but this may or may not be useful depending on the
559 scales that one is interested in.

560 **Acknowledgments**

561 This material is based upon work supported by, or in part by, the US
562 Army Research Office under Contract/Grant number W911NF-18-1-0338.
563 The authors were also supported by the National Science Foundation under
564 awards EAR-1351623 and EAR-1417264, EAR-1446236, and CBET-1705770.

- 565 [1] J. Bear, Dynamics of fluids in porous media, Courier Corporation, 2013.
- 566 [2] J. Salles, J.-F. Thovert, R. Delannay, L. Prevors, J.-L. Auriault,
567 P. Adler, Taylor dispersion in porous media. determination of the dis-
568 persion tensor, *Physics of Fluids A* 5 (10) (1992) 2348–2376.
- 569 [3] D. Lester, G. Metcalfe, M. Trefry, Anomalous transport and chaotic ad-
570 vection in homogeneous porous media, *Physical Review E* 90 (6) (2014)
571 063012.
- 572 [4] M. Maghrebi, I. Jankovic, R. M. Allen-King, A. J. Rabideau, I. Kali-
573 novich, G. S. Weissmann, Impacts of transport mechanisms and plume
574 history on tailing of sorbing plumes in heterogeneous porous formations,
575 *Advances in water resources* 73 (2014) 123–133.
- 576 [5] M. Maghrebi, I. Jankovic, G. S. Weissmann, L. S. Matott, R. M. Allen-
577 King, A. J. Rabideau, Contaminant tailing in highly heterogeneous
578 porous formations: Sensitivity on model selection and material prop-
579 erties, *Journal of Hydrology* 531 (2015) 149–160.
- 580 [6] G. Taylor, Dispersion of soluble matter in solvent flowing slowly through
581 a tube, *Proceedings of the Royal Society of London. Series A*, 219 (1953)
582 186–203 186–203.
- 583 [7] R. Aris, On the dispersion of solute in a fluid flowing through a tube,
584 *Proceedings of the Royal Society of London. Series A*, 235 (1956) 67–77.
- 585 [8] H. Brenner, Dispersion resulting from flow through spatially periodic
586 porous media, *Philosophical Transactions of the Royal Society of Lon-
587 don. Series A* 297 (1980) 81–133.

- 588 [9] O. Plumb, S. Whitaker, Dispersion in heterogeneous porous media: 1.
589 local volume averaging and large-scale averaging, *Water Resources Re-*
590 *search* 24 (1988) 913–926.
- 591 [10] U. Hornung, *Homogenization and Porous Media*, Springer, 1997.
- 592 [11] M. Shapiro, H. Brenner, Dispersion of a chemically reactive solute in
593 a spatially periodic model of a porous medium, *Chemical Engineering*
594 *Science* 43 (3) (1988) 551–571.
- 595 [12] B. Dykaar, P. Kitanidis, Macrotransport of a biologically reacting solute
596 through porous media, *Water Resources Research* 32 (1996) 307–329.
- 597 [13] D. Bolster, F. Valdes-Parada, T. L. Borgne, M. Dentz, J. Carrera, Mix-
598 ing in confined stratified aquifers, *Journal of Contaminant Hydrology*
599 120-121 (2011) 198–212.
- 600 [14] M. Levesque, O. Bénichou, R. Voituriez, B. Rotenberg, Taylor dispersion
601 with adsorption and desorption, *Physical Review E* 86 (3) (2012) 036316.
- 602 [15] L. Zhang, M. A. Hesse, M. Wang, Transient solute transport with sorp-
603 tion in poiseuille flow, *Journal of Fluid Mechanics* 828 (2017) 733–752.
604 doi:10.1017/jfm.2017.546.
- 605 [16] I. Battiato, D. M. Tartakovsky, A. M. Tartakovsky, T. Scheibe, On
606 breakdown of macroscopic models of mixing-controlled heterogeneous
607 reactions in porous media, *Advances in Water Resources* 32 (11) (2009)
608 1664–1673.

- 609 [17] I. Battiato, D. Tartakovsky, Applicability regimes for macroscopic mod-
610 els of reactive transport in porous media, *Journal of Contaminant Hy-*
611 *drology* 120 (2011) 18–26.
- 612 [18] K. Rehfeldt, J. Boggs, L. Gelhar, Field study of dispersion in a het-
613 erogeneous aquifer. 3: Geostatistical analysis of hydraulic conductivity,
614 *Water Resources Research* 28 (1992) 3309–3324.
- 615 [19] C. Harvey, S. M. Gorelick, Rate-limited mass transfer or macrodispers-
616 ion: Which dominates plume evolution at the macrodispersion experi-
617 ment (made) site?, *Water Resources Research* 36 (3) (2000) 637–650.
- 618 [20] A. Cortis, B. Berkowitz, Anomalous transport in “classical” soil and
619 sand columns, *Soil Science Society of America Journal* 68 (5) (2004)
620 1539–1548.
- 621 [21] M. Dentz, A. Cortis, H. Scher, B. Berkowitz, Time behavior of solute
622 transport in heterogeneous media: transition from anomalous to normal
623 transport, *Advances in Water Resources* 27 (2) (2004) 155–173.
- 624 [22] Y. Zhang, D. A. Benson, B. Baeumer, Predicting the tails of break-
625 through curves in regional-scale alluvial systems, *Groundwater* 45 (4)
626 (2007) 473–484.
- 627 [23] M. C. Richmond, W. A. Perkins, T. D. Scheibe, A. Lambert, B. D.
628 Wood, Flow and axial dispersion in a sinusoidal-walled tube: Effects of
629 inertial and unsteady flows, *Advances in Water Resources*.
- 630 [24] M. L. Porter, F. J. Valdés-Parada, B. D. Wood, Comparison of theory

- 631 and experiments for dispersion in homogeneous porous media, *Advances*
632 *in Water Resources* 33 (9) (2010) 1043–1052.
- 633 [25] G. Porta, G. Ceriotti, J.-F. Thovert, Comparative assessment of
634 continuum-scale models of bimolecular reactive transport in porous me-
635 dia under pre-asymptotic conditions, *Journal of contaminant hydrology*
636 185 (2016) 1–13.
- 637 [26] Y. Davit, B. D. Wood, G. Debenest, M. Quintard, Correspondence be-
638 tween one-and two-equation models for solute transport in two-region
639 heterogeneous porous media, *Transport in porous media* 95 (1) (2012)
640 213–238.
- 641 [27] T. L. Borgne, M. Dentz, J. Carrera, Lagrangian statistical model for
642 transport in highly heterogeneous velocity fields, *Physical Review Let-*
643 *ters* 101 (2008) 090601.
- 644 [28] N. L. Sund, D. Bolster, D. A. Benson, Testing the limits of the spatial
645 markov model for upscaling transport: The role of nonmonotonic effec-
646 tive velocity autocorrelations, *Physical Review E* 94 (4) (2016) 043107.
- 647 [29] B. Berkowitz, A. Cortis, M. Dentz, H. Scher, Modeling non-Fickian
648 transport in geological formations as a continuous time random walk,
649 *Reviews of Geophysics* 44 (2).
- 650 [30] D. Bolster, Y. Méheust, T. Le Borgne, J. Bouquain, P. Davy, Model-
651 ing preasymptotic transport in flows with significant inertial and trap-
652 ping effects—the importance of velocity correlations and a spatial Markov
653 model, *Advances in Water Resources* 70 (2014) 89–103.

- 654 [31] T. L. Borgne, M. Dentz, J. Carrera, Spatial Markov processes for model-
655 ing Lagrangian particle dynamics in heterogeneous porous media, *Physical Review E* 78 (2008) 026308.
656
- 657 [32] P. K. Kang, M. Dentz, T. Le Borgne, R. Juanes, Spatial Markov model of
658 anomalous transport through random lattice networks, *Physical Review*
659 *Letters* 107 (18) (2011) 180602.
- 660 [33] T. Le Borgne, D. Bolster, M. Dentz, P. Anna, A. Tartakovsky, Effec-
661 tive pore-scale dispersion upscaling with a correlated continuous time
662 random walk approach, *Water Resources Research* 47 (12).
- 663 [34] P. De Anna, T. Le Borgne, M. Dentz, A. M. Tartakovsky, D. Bolster,
664 P. Davy, Flow intermittency, dispersion, and correlated continuous time
665 random walks in porous media, *Physical Review Letters* 110 (18) (2013)
666 184502.
- 667 [35] P. K. Kang, P. Anna, J. P. Nunes, B. Bijeljic, M. J. Blunt, R. Juanes,
668 Pore-scale intermittent velocity structure underpinning anomalous
669 transport through 3-d porous media, *Geophysical Research Letters*
670 41 (17) (2014) 6184–6190.
- 671 [36] N. Sund, D. Bolster, S. Mattis, C. Dawson, Pre-asymptotic transport
672 upscaling in inertial and unsteady flows through porous media, *Trans-*
673 *port in Porous Media* 109 (2) (2015) 411–432.
- 674 [37] P. K. Kang, T. Le Borgne, M. Dentz, O. Bour, R. Juanes, Impact of
675 velocity correlation and distribution on transport in fractured media:
676 Field evidence and theoretical model, *Water Resources Research*.

- 677 [38] N. L. Sund, D. Bolster, C. Dawson, Upscaling transport of a react-
678 ing solute through a periodically converging–diverging channel at pre-
679 asymptotic times, *Journal of contaminant hydrology* 182 (2015) 1–15.
- 680 [39] N. Sund, G. Porta, D. Bolster, R. Parashar, A lagrangian transport
681 eulerian reaction spatial (laters) markov model for prediction of effective
682 bimolecular reactive transport, *Water Resources Research* 53 (11) (2017)
683 9040–9058.
- 684 [40] N. L. Sund, G. M. Porta, D. Bolster, Upscaling of dilution and mixing
685 using a trajectory based spatial markov random walk model in a periodic
686 flow domain, *Advances in Water Resources* 103 (2017) 76–85.
- 687 [41] T. Bahar, F. Golfier, C. Oltéan, E. Lefevre, C. Lorgeoux, Com-
688 parison of theory and experiment for npl dissolution in porous
689 media, *Journal of Contaminant Hydrology* 211 (2018) 49–64.
690 doi:10.1016/j.jconhyd.2018.03.004.
- 691 [42] G. Boccardo, E. Crevacore, R. Sethi, M. Icardi, A robust upscaling of the
692 effective particle deposition rate in porous media, *Journal of Contami-
693 nant Hydrology* 212 (2018) 3–13. doi:10.1016/j.jconhyd.2017.09.002.
- 694 [43] P. K. Kang, S. Brown, R. Juanes, Emergence of anomalous transport
695 in stressed rough fractures, *Earth and Planetary Science Letters* 454
696 (2016) 46–54.
- 697 [44] T. Sherman, A. Fakhari, S. Miller, K. Singha, D. Bolster, Parameterizing
698 the spatial markov model from breakthrough curve data alone, *Water
699 Resources Research* 53 (12) (2017) 10888–10898.

- 700 [45] T. Sherman, A. Foster, D. Bolster, K. Singha, Predicting downstream
701 concentration histories from upstream data in column experiments, *Water
702 Resources Research* ?? (2018) Under Review.
- 703 [46] B. Rathi, H. Neidhardt, M. Berg, A. Siade, H. Prommer, Processes
704 governing arsenic retardation on pleistocene sediments: Adsorption ex-
705 periments and model-based analysis, *Water Resources Research* 53 (5)
706 (2017) 4344–4360. doi:10.1002/2017WR020551.
- 707 [47] O. Iliev, Z. Lakdawala, K. Neßler, T. Prill, Y. Vutov, Y. Yang, J. Yao,
708 On the pore-scale modeling and simulation of reactive transport in 3d
709 geometries, *Mathematical Modelling and Analysis* 22 (5) (2017) 671–
710 694. doi:10.3846/13926292.2017.1356759.
- 711 [48] C. da Luz, S. de Arruda Guelli Ulson de Souza, A. Ulson de Souza,
712 A. Dervanoski, A. de Oliveira Samel Moraes, B. Wood, A multiscale
713 model for carbon adsorption of btx compounds: Comparison of volume
714 averaging theory and experimental measurements, *Chemical Engineer-
715 ing Science* 184 (2018) 285–308. doi:10.1016/j.ces.2018.02.047.
- 716 [49] N. Seetha, M. Mohan Kumar, S. Majid Hassanizadeh, A. Raoof, Virus-
717 sized colloid transport in a single pore: Model development and sensi-
718 tivity analysis, *Journal of Contaminant Hydrology* 164 (2014) 163–180.
719 doi:10.1016/j.jconhyd.2014.05.010.
- 720 [50] Y. Edery, A. Guadagnini, H. Scher, B. Berkowitz, Origins of anomalous
721 transport in heterogeneous media: Structural and dynamic controls,
722 *Water Resources Research* 50 (2) (2014) 1490–1505.

- 723 [51] K. Chaudhary, M. Cardenas, W. Deng, P. Bennett, Pore geometry ef-
724 fects on intrapore viscous to inertial flows and on effective hydraulic
725 parameters, *Water Resources Research* 49 (2013) 1149–1162.
- 726 [52] K. Chaudhary, M. B. Cardenas, W. Deng, P. C. Bennett, The role of
727 eddies inside pores in the transition from Darcy to Forchheimer flows,
728 *Geophysical Research Letters* 38 (24).
- 729 [53] J. Bouquain, Y. Meheust, D. Bolster, P. Davy, The impact of inertial
730 effects on solute dispersion in a channel with periodically varying aper-
731 ture, *Physics of Fluids* 24 (2012) 083602.
- 732 [54] M. B. Cardenas, Direct simulation of pore level Fickian dispersion
733 scale for transport through dense cubic packed spheres with vortices,
734 *Geochem., Geophys., Geosyst.* 10 (2009) Q12014.
- 735 [55] D. Bolster, T. L. Borgne, M. Dentz, Solute dispersion in channels with
736 periodically varying apertures, *Physics of Fluids* 21 (2009) 056601.
- 737 [56] M. B. Cardenas, Three-dimensional vortices in single pores and their
738 effects on transport, *Geophysical Research Letters* 35 (18).
- 739 [57] T. LeBorgne, D. Bolster, M. Dentz, P. de Anna, A. Tartakovsky, Effec-
740 tive pore-scale dispersion upscaling with a correlated CTRW approach,
741 *Water Resources Research* 47 (2012) W12538.
- 742 [58] P. Kitanidis, B. Dykaar, Stokes flow in a slowly varying two-dimensional
743 periodic pore, *Transport in Porous Media* 26 (1997) 89–98.

- 744 [59] J. Cao, P. Kitanidis, Adaptive finite element simulation of stokes flow
745 in porous media, *Advances in water resources* 22 (1) (1998) 17–31.
- 746 [60] M. Khan, Non-equilibrium theory of capillary columns and the effect of
747 interfacial resistance on column efficiency, *Gas Chromatography* (1962)
748 3–17.
- 749 [61] T. Ptak, G. Teutsch, Forced and natural gradient tracer tests in a
750 highly heterogeneous porous aquifer: instrumentation and measure-
751 ments, *Journal of Hydrology* 159 (1-4) (1994) 79–104.
- 752 [62] V. L. Morales, M. Dentz, M. Willmann, M. Holzner, Stochastic dynamics
753 of intermittent pore-scale particle motion in three-dimensional porous
754 media: Experiments and theory, *Geophysical Research Letters* 44 (18)
755 (2017) 9361–9371.
- 756 [63] M. Dentz, P. K. Kang, A. Comolli, T. Le Borgne, D. R. Lester, Con-
757 tinuous time random walks for the evolution of lagrangian velocities,
758 *Physical Review Fluids* 1 (7) (2016) 074004.
- 759 [64] A. Comolli, M. Dentz, Anomalous dispersion in correlated porous me-
760 dia: a coupled continuous time random walk approach, *The European*
761 *Physical Journal B* 90 (9) (2017) 166.
- 762 [65] P. K. Kang, M. Dentz, T. Le Borgne, S. Lee, R. Juanes, Anomalous
763 transport in disordered fracture networks: spatial markov model for
764 dispersion with variable injection modes, *Advances in Water Resources*
765 106 (2017) 80–94.

- 766 [66] H. Risken, Fokker-Planck Equation, Springer, 1984.
- 767 [67] G. Boccardo, I. M. Sokolov, A. Paster, An improved scheme for a robin
768 boundary condition in discrete-time random walk algorithms, Journal
769 of Computational Physics 374 (2018) 1152–1165.
- 770 [68] E. Wright, N. Sund, D. Richter, G. Porta, D. Bolster, Upscaling mixing
771 in highly heterogeneous porous media via a spatial markov model, Water
772 11 (1) (2019) 53.
- 773 [69] S. Most, Analysis and simulation of anomalous transport in porous me-
774 dia, Ph.D. thesis, University of Stuttgart (2019).
- 775 [70] A. Massoudieh, M. Dentz, J. Alikhani, A spatial markov model for
776 the evolution of the joint distribution of groundwater age, arrival time,
777 and velocity in heterogeneous media, Water Resources Research 53 (7)
778 (2017) 5495–5515.